

The O 1s and V 2p X-ray Absorption Spectra of Vanadium Oxides

M. Abbate*

Solid State Spectroscopy, University of Nijmegen
Toernooiveld 1, 6525 ED Nijmegen, The Netherlands

Received March 3, 1994

We present and discuss the O 1s and V 2p X-ray absorption spectra (XAS) of several vanadium oxides with different formal valences and chemical environments. The O 1s XAS spectra reflect the unoccupied electronic states in the conduction band and provide very useful information on crystal-field splitting, band width and hybridization strength. The O 1s XAS spectrum of VO₂ in the metallic phase is properly reproduced by an O p partial density of unoccupied states calculated with the localized-spherical-wave method. The O 1s XAS spectra of VO₂ taken at 300 K (semiconducting phase) and 390 K (metallic phase) show clearly the splitting of the V 3d bands across the semiconductor-metal transition ($T_c \approx 340K$). The V 2p XAS spectra present significant multiplet effects and chemical shifts which provide very helpful information on the character and symmetry of the ground state. The V 2p XAS spectrum of V₂O₃ is precisely simulated by an atomic-multiplet calculation projected on the appropriate crystal-field. The V 2p XAS spectra of the (Li,Zn) V₂O₄ series present clear chemical shifts and considerable changes in the shape of the multiplets. These effects denote a change in the character of the ground state and show that the holes induced by Li substitution in ZnV₂O₄ contain mainly V 3d character.

I. Introduction

The purpose of this paper is to illustrate the potential of soft X-ray absorption spectroscopy (XAS) in the study of the electronic structure of transition-metal oxides. To this end, we present and discuss the O 1s and V 2p XAS spectra of several vanadium oxides with different formal valences and chemical environments. These materials were selected among many others transition-metal oxides because they present particularly interesting electric and magnetic properties. Most of the experimental studies done up till now on these materials were concerned with diverse electron and X-ray spectroscopy techniques which probe occupied electronic states. However, there is a real need for complementary studies of the unoccupied electronic states because these states include a major part of the significant V 3d bands. We show below that soft XAS can play a leading role in this area by providing information on the ground state, band dispersion, metal-ligand hybridization and crystal-field effects. For in-

stance, XAS reflects clearly the changes in the V 3d bands across the metal-insulator transition of VO₂. In addition, XAS shows convincingly that the holes induced by Li substitution in ZnV₂O₄ contain mainly V 3d character.

The oxygen chemistry of vanadium is particularly rich and leads to compounds with very interesting physical and chemical properties^[1]. The series V₂O₃, VO₂ and V₂O₅, for example, contains vanadium ions in different formal valences and chemical environments. These binary oxides present a broad range of electric and magnetic properties, which include very interesting metal-insulator transitions as a function of temperature^[2-4]. For instance, V₂O₃ undergoes a first order transition at $T_c \approx 150K$ from an antiferromagnetic semiconductor phase at low temperature to a paramagnetic metallic state above T_c . In the metallic state, V₂O₃ presents the corundum structure (Al₂O₃) with strong metal-metal interactions along the hexagonal c-axis as well as in the basal plane. Next, VO₂ undergoes a first order transition at $T_c \approx 340K$ from a diamagnetic semiconductor phase at low temperature

*Present Address: Laboratório Nacional de Luz Síncrotron, CNPq, Caixa Postal 6192, 13081 Campinas SP, Brazil.

to a paramagnetic metallic state above T_c . In the metallic state, VO_2 presents the rutile structure (TiO_2) with strong metal-metal interactions along the rutile c-axis. Finally, V_2O_5 is a diamagnetic insulator and presents an orthorhombic structure. The oxygen coordination around the V ions in V_2O_5 deviates from the ideal octahedra and direct metal-metal interactions are very weak.

In addition to these binary oxides, there are several ternary oxide series with very interesting physical properties. For example, the $\text{Li}_x\text{Zn}_{1-x}\text{V}_2\text{O}_4$ series present the spinel structure (MgAl_2O_4) and exhibit a metal-insulator transition as a function of composition. The parent compound ZnV_2O_4 is an antiferromagnetic insulator and becomes a highly correlated paramagnetic metal when approximately 35% of Zn is replaced by Li^[5,6,7].

These materials have attracted considerable attention from both experimental and theoretical viewpoints. For example, the electronic structure of vanadium oxides were studied using different band-structure^[8-10] and cluster-model calculations^[11,12]. The origin and the character of the metal-insulator transitions were often discussed in terms of model calculations^[13-15]. Several series of vanadium oxides were investigated by means of core-level X-ray photoelectron spectroscopy (XPS)^[16-18]. The conduction bands of V_2O_3 were analyzed using angle-resolved and resonant photoemission^[19,20]. The electronic structure and the metal-insulator transition of related vanadium oxides were probed by means of reflectance and photoemission spectroscopy^[21]. The XAS spectra of several vanadium oxides were already reported in Ref. 22. Finally, the electronic structure and the metal-insulator transition of $\text{Li}_x\text{Zn}_{1-x}\text{V}_2\text{O}_4$ were studied by photoemission spectroscopy^[23].

II. X-ray absorption spectroscopy

In the soft X-ray absorption process, a shallow core-level electron absorbs a photon and is excited to unoccupied electronic states above the Fermi level^[24]. The X-ray absorption mechanism within the single particle approximation is illustrated schematically in Fig. 1a. The transition probability for the XAS process σ can

be calculated by using the *Golden Rule*

$$\sigma(h\nu) \propto \sum_i |\langle \Psi_f | \mathbf{A} \mathbf{p} | \Psi_i \rangle|^2 \delta(h\nu - E_f + E_i), \quad (1)$$

where $|\Psi_f\rangle$ is the final state, $|\Psi_i\rangle$ is the initial state. \mathbf{A} is the electromagnetic vector potential, \mathbf{p} is the momentum operator acting on the active electron, $h\nu$ is the photon energy, E_f is the final state energy, E_i is the initial state energy and the sum runs over all the possible final states. The angular part of the matrix element gives rise to the well known *dipole selection rule* ($\Delta l = \pm 1$). In addition, the matrix element is sensitive only to local states because the radial part involves a core-level electron. This means that XAS probes site- and symmetry-selected unoccupied electronic states. In particular, the O 1s XAS spectra probe unoccupied O 2p states and the V 2p XAS spectra probe mostly unoccupied V 3d character^[25].

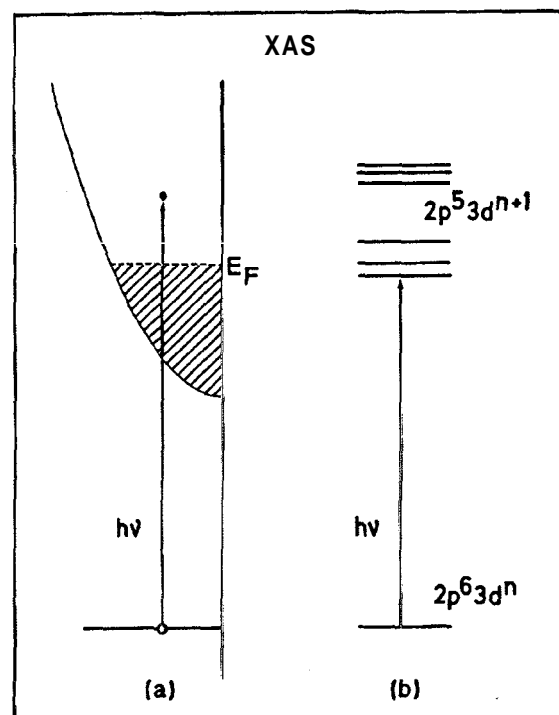


Figure 1: (a) Schematic representation of the soft X-ray absorption process within the single particle approximation. (b) Soft X-ray absorption process between the initial and one of the possible final states in the transition-metal 2p edges.

There are two extreme regimes in soft XAS which depend on the relative magnitude of intra-atomic interactions versus the dispersion of the ensuing final state band. In the first regime, the multipole interactions are small compared to the band width and the independent

particle approach is a good starting point for the interpretation of the spectra. The transition probability in this regime is given by

$$\sigma(h\nu) \propto \sum_i |\langle \phi_f | \mathbf{A} \mathbf{p} | \phi_i \rangle|^2 \delta(h\nu - E_f + E_i), \quad (2)$$

where $|\phi_f\rangle$ and $|\phi_i\rangle$ refer now to the active electron. In a first approximation, the matrix element M does not depend very strongly on the final state and can be taken out of the sum. The sum over the possible final states of the delta function gives a partial density of states and the transition probability becomes

$$\sigma(h\nu) \propto |M|^2 P_i(h\nu - E_f + E_i), \quad (3)$$

where P_i corresponds to the local density of unoccupied states projected on the appropriate angular momentum l . This means that the shape of the spectra in this regime is directly related to the partial density of states. The density of unoccupied states can be routinely obtained from standard band-structure calculations. This approach gives reasonable good results for the O 1s XAS spectra of many transition-metal oxides.

In the second regime, the interactions between the core-hole and the valence electrons dominate and the spectra must be interpreted in terms of transitions from a well defined ground state to a set of possible excited states, as illustrated in Fig. 1b. The transition probability in this case is given by:

$$\sigma(h\nu) \propto \sum_i |\langle 2p^5 3d^{n+1} | \mathbf{A} \mathbf{p} | 2p^6 3d^n \rangle|^2 \delta(h\nu - E_f + E_i), \quad (4)$$

where both the $|2p^6 3d^n\rangle$ and the $|2p^5 3d^{n+1}\rangle$ states include explicitly the dominant 2p core-level electrons. In this case, the spectra present strong multiplet effects which are caused by relatively large Coulomb and exchange interactions. The spectra can be explained by atomic-like calculations projected on the appropriate crystal-field. The atomic-like transition lines are then convoluted with a Gaussian function to take into account the dispersion of the metal-3d bands. The precise shape of the multiplets in this case is directly related to the symmetry of the ground state and the strength of the crystal-field splitting. This approach gives very good results for the metal 2p X-ray absorption spectra of most transition-metal compounds.

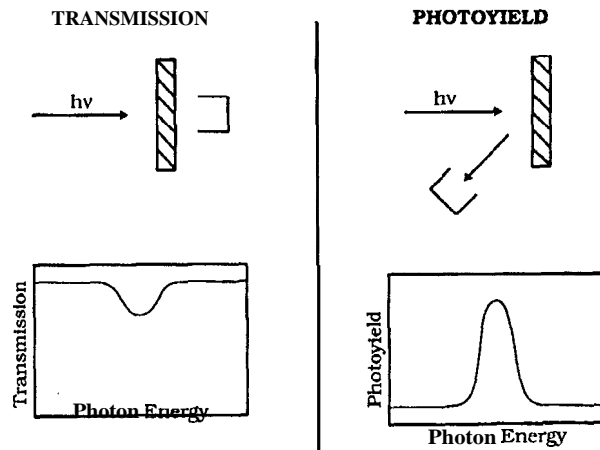


Figure 2: Schematic representation of the experimental methods used to measure X-ray absorption spectra: Transmission mode (left panel) and Photoyield mode (right panel).

The hard X-ray absorption spectra are usually taken in transmission mode by measuring the attenuation of the X-ray beam after a thin film, as illustrated in the left panel of Fig. 2. This method is very well suited for hard X-rays because the penetration depths are rather long and thin films of the appropriate thickness can be easily produced. However, for soft X-rays with energies below 2 keV, the mean absorption length near the threshold is very short and it is very difficult to produce good quality films of the appropriate thickness. Fortunately, it was found that the total-electron-yield from a sample is very often directly proportional to the X-ray absorption cross section^[26]. This acquisition method is illustrated schematically in the right panel of Fig. 2. The only restriction of this method is that the escape depth of the emitted electrons must be short by comparison to the mean absorption length. The mean-probing-depth of X-ray absorption spectroscopy measured in total-electron-yield mode is in the 20-50 Å range^[27].

III. Experimental results

The V_2O_3 , VO_2 and V_2O_5 samples were single crystals grown by the chemical-vapor-transport method. The X-ray absorption spectra of these samples were taken at the NSLS in Brookhaven by using the Dragon monochromator^[28,29]. The energy resolution of the monochromator at the O 1s and V 2p absorption edges (around 510-555 eV) was set to approximately

250 meV. The samples were glued to the sample-holder using a silver epoxy to ensure a good electrical and thermal contact. The VO_2 sample was heated by an electric resistance device and the temperature was measured with a diode sensor. The base pressure in the main chamber was in the low 10^{-10} Torr range. The spectra were collected using the total-electron-yield mode and normalized to the maximum peak intensity.

The $\text{Li}_x\text{Zn}_{1-x}\text{V}_2\text{O}_4$ samples were sintered pellets obtained by repeated cycles of grinding, mixing, pressing and firing in oxygen atmosphere. The samples were then analyzed by means of X-ray diffraction to rule out the presence of impurity phases. The XAS spectra of these samples were taken at BESSY in Berlin by using the SX700-II monochromator^[30]. The energy resolution of the monochromator in the 510-555 eV energy range was set to approximately 250 meV. The base pressure in the measurement chamber was better than 5×10^{-10} Torr. The samples were introduced to the analysis chamber by means of a fast-entry-lock system to avoid possible oxygen losses during the bake-out. The spectra were collected using the total-electron-yield mode, divided by the yield of clean platinum to take into account the throughput of the monochromator and normalized to the maximum intensity.

IV. Results and discussion

A. O 1s XAS spectra of V_2O_3 , VO_2 and V_2O_5

The O 1s X-ray absorption spectra of V_2O_3 , VO_2 and V_2O_5 are shown in Fig. 3. The spectra correspond to transitions from the O 1s core-level to unoccupied O p character mixed in the conduction band. The absorption intensity, which should be very weak in a purely ionic picture, provides a good indication of covalence effects^[31]. The different features in the spectra correspond to bands of primary metal character. The main character of each band can be inferred from the parent molecular-orbital levels^[32-34], as illustrated in the top part of Fig. 4. The prominent doublets near the edge (around 530-537 eV) are attributed to V 3d bands which are split by crystal-field effects. The broader structures at higher energies (around 537-550 eV) are attributed to V 4sp bands. The V 4sp bands appear at

higher energies because of the relatively larger V 4sp-O 2p antibonding interactions.

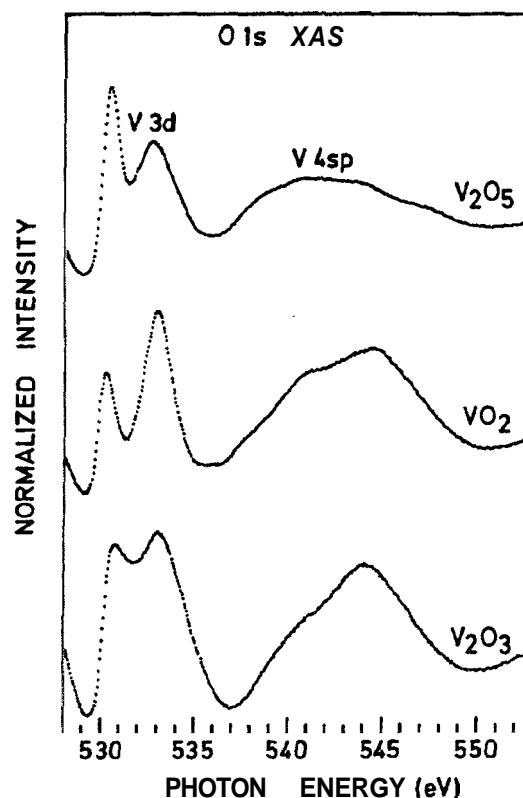


Figure 3: O 1s X-ray absorption spectra of V_2O_3 , VO_2 and V_2O_5 .

The splitting of the V 3d bands observed in the O 1s XAS spectra is caused by crystal-field effects. The splitting of the V 3d levels is illustrated schematically in the bottom part of Fig. 4. The origin of these splittings can be qualitatively explained in terms of symmetry considerations^[35,36]. The upper band (e_g levels) corresponds to V 3d orbitals which point towards the ligands. These states appear at higher energies because they form relatively stronger σ antibonding combinations with O 2p orbitals. On the other hand, the lower band (t_{2g} levels) corresponds to orbitals which point in between the ligands. These states have a smaller overlap with ligand sites and form weaker π antibonding combinations.

The intensity of the different structures in the O 1s spectra are related to the strength of the metal-ligand hybridization in each molecular-orbital derived band. Fig. 3 shows that the relative intensity of the V 3d bands increases with respect to the V 4sp bands as one

goes from V_2O_3 to V_2O_5 . This relative enhancement is not only related to more V 3d unoccupied character, but also to a larger V 3d-O 2p hybridization for higher V valences. This trend indicates also that the covalent contribution to the chemical bonding of the V 3d electrons increases from V_2O_3 to V_2O_5 .

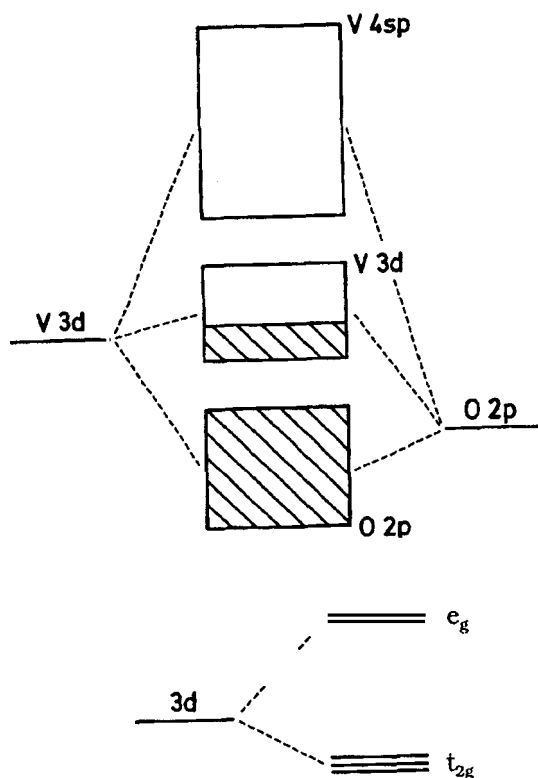


Figure 4: Schematic representation of the electronic structure of vanadium oxides in terms of MO derived bands (above). The V 3d levels are split into t_{2g} and e_g components by crystal-field effects (below).

Fig. 3 shows also that the V 3d bands of V_2O_3 are broader than those of VO_2 and V_2O_5 . The broadening in the spectra is mainly given by the dispersion of the V 3d bands^[37]. Part of the V 3d dispersion in these oxides is given by indirect interactions via the ligands (V 3d-O 2p-V 3d). This mechanism explains why the e_g band, which is related to stronger V 3d-O 2p σ bonds, is usually broader than the t_{2g} band, which is related to weaker V 3d-O 2p π bonds. The extra broadening in the case of V_2O_3 is attributed to particularly large V 3d-V 3d interactions caused by the relatively short V-V distances in this compound.

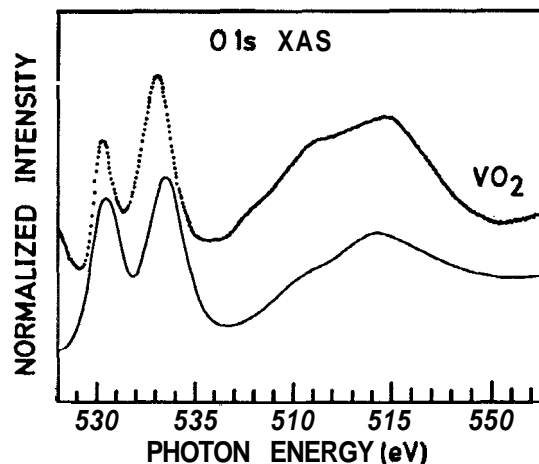


Figure 5: Comparison between the experimental O 1s X-ray absorption spectrum of VO_2 in the metallic phase (dots) and a partial density of unoccupied states projected on O p symmetry calculated by means of the LSW method (solid line).

Fig. 5 compares the O 1s spectrum of VO_2 in the metallic phase and a broadened O p density of unoccupied states (DOS). The partial DOS was calculated using the localized-spherical-wave (LSW) method with an extended basis set^[38,39]. The theoretical result was shifted by hand to get the best overall match with the experimental spectrum. The agreement between theory and experiment is very good over the whole spectral range. This shows that band structure calculations can give reasonable results for the O 1s XAS spectra of some early transition-metal oxides. This is somewhat unexpected and even puzzling because the 3d-3d interactions in these compounds cannot be neglected. A more accurate analysis should also take into account the energy dependence of the matrix-elements, self-energy effects^[40] and the core-hole potential^[41].

B. The metal-insulator transition of VO_2

Fig. 6 shows the O 1s soft X-ray absorption spectra of VO_2 taken at 300 K (semiconductor phase) and at 390 K (metallic phase)^[42]. The main interest here concerns the changes in the electronic structure of VO_2 across the phase transition. Only the V 3d band regions are shown because the V 4sp bands show hardly any change as a function of temperature. The origin of the different peaks in the spectra can be explained in terms of molecular-orbital (MO) and crystal-field ideas proposed by Goodenough^[43].

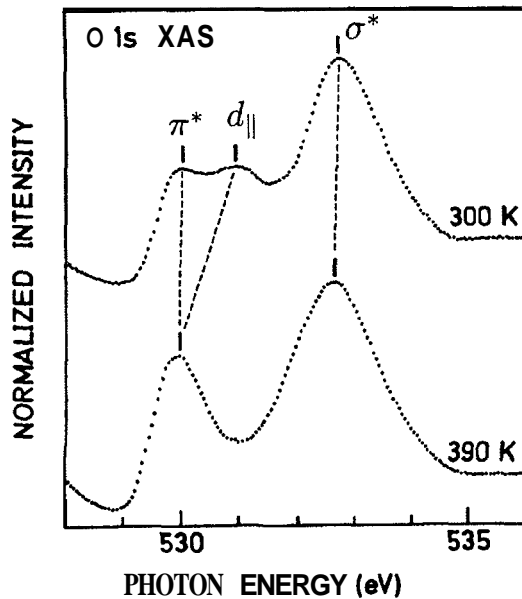


Figure 6: O 1s X-ray absorption spectra of VO₂ taken at 300 K (semiconductor phase) and at 390 K (metallic phase). The different peaks in the spectra are labeled according to the approximate MO classification scheme.

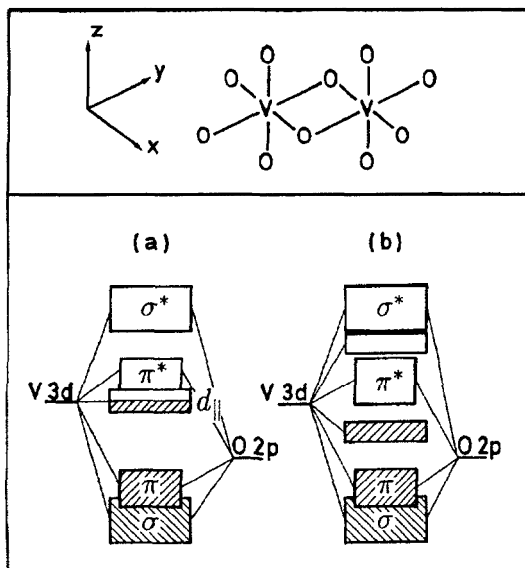


Figure 7: Schematic representation of the VO₆ octahedras in the undistorted rutile structure (top panel). Electronic structure of VO₂ in terms of the MO derived bands (lower panel): (a) undistorted structure (metallic phase) and (b) distorted structure (semiconductor phase).

The top panel of Fig. 7 shows how the VO₆ octahedras share edges in the undistorted rutile structure (metallic phase). In this coordinate system, the V 3d orbitals of $3z^2 - r^2$ and $x^2 - y^2$ symmetry point towards the ligands and form σ bands with the O 2p orbitals. Next, the orbitals of xz and yz symmetry point in between the ligands and form π bands. Finally, the xy orbitals point towards the next-nearest-neighbor V site

and form the d_{\parallel} band. The schematic electronic structure of metallic VO₂ based on this MO analysis is shown in Fig. 7a. The metallic behavior is the consequence of the partially filled d_{\parallel} band overlapping the π^* bands. In the semiconductor phase below T_c , a local distortion forms pairs of V atoms changing the crystallographic structure. The electronic interactions within the V-V pairs split the d_{\parallel} band into two components, as illustrated in Fig. 7(b). The filling of the lower band, which corresponds to a singlet formation within the V-V pairs, explains both the drop of the electric conductivity and the absence of magnetic moments below T_c .

The different peaks in the O 1s XAS spectra are labeled according to this approximate MO classification scheme, see Fig. 6. The band-structure effects and the electron repulsion interactions within the V-V pairs are strong enough to push the unoccupied part of the d_{\parallel} band approximately 1 eV above the π^* bands edge. By contrast, the weaker shift of the σ^* bands (approximately 0.2 eV) reflects smaller electron-lattice interactions and the relatively non-bonding π^* bands hardly shift at all. Optical data and photoemission spectra indicate that the band gap in the insulator phase is approximately 0.7 eV^[21]. This band gap used in combination with the present results gives a splitting of approximately 2 eV between the lower and upper d_{\parallel} bands. In conclusion, the main change in the electronic structure of VO₂ across the metal-insulator transition occurs in the d_{\parallel} band.

The changes in the electronic structure of VO₂ are caused by both electron-electron repulsion and electron-lattice interactions. On the one hand, band-structure calculations can partially explain the band gap opening in terms of the reduced symmetry and the ensuing changes in the hybridization^[8-10]. On the other hand, cluster-model calculations suggest that electron correlation effects contribute approximately 0.7-0.9 eV to the splitting of the d_{\parallel} band^[11,12]. In fact, it is very difficult to explain the large splitting of the d_{\parallel} band in terms of band-structure effects alone. Finally, we note that the metal-insulator transition in VO₂ is basically driven by the decrease in the electronic contribution to the energy caused by the filling of the lower d_{\parallel} band.

C. V 2p XAS spectra of V_2O_3 , VO_2 and V_2O_5

The V 2p X-ray absorption spectra of V_2O_3 , VO_2 and V_2O_5 are shown in Fig. 8. The spectra correspond to transitions from a well defined ground state $|2p^63d^n\rangle$ to one of the possible final states $|2p^53d^{n+1}\rangle$ allowed by the dipole selection rule. The spectra show two broad structures (around 518 and 525 eV approximately) which can be attributed, in a first approximation, to the $2p_{3/2}$ and $2p_{1/2}$ core-levels respectively. However, the interactions between the core-hole and the valence electrons in the final state are of the order of the spin-orbit splitting of the 2p level. The breakdown of the jj coupling scheme causes a noticeable redistribution of the spectral weight throughout the entire spectra. In addition, the V 2p-3d and 3d-3d Coulomb and exchange interactions are large in comparison to the dispersion of the 3d bands, which causes strong multiplet effects.

The V 2p spectra present noticeable chemical shifts and the shape of the multiplets is completely different, see Fig. 8. These changes provide interesting information on the electronic structure of these materials. The chemical shifts are caused by changes in the average electrostatic energy at the vanadium sites and are characteristic of the different vanadium valences in the series^[44]. In particular, the V 2p peaks shift to higher energies for those compounds with vanadium ions in a higher formal valence state. The shape of the spectra is dictated by the set of final states which can be reached from the ground state via the dipole selection rule^[45]. This means that the multiplets observed in the V 2p spectra depend directly on the symmetry of the ground state^[46,47]. This dependence was used to study the changes in the electronic structure of transition-metal compounds induced by substitution and doping^[48,49].

The experimental V 2p XAS spectrum of V_2O_3 is compared in Fig. 9 to an atomic-multiplet calculation projected in octahedral symmetry. The theoretical spectrum was calculated assuming a $t_{2g}^2(^3T_1)$ ground state, the Slater integrals scaled down to 80% of their Hartree-Fock values and the crystal-field strength parameter $10 Dq$ set to 1.5 eV. The calculated spectrum was broadened with a Gaussian and a Lorentzian functions to take into account the experimental resolution

and the lifetime broadening respectively. In addition, the simulation was shifted by hand to get the best overall agreement with the experiment. The match is very good and illustrates the potential of soft XAS to determine the symmetry of the ground state. A more accurate analysis should take into account the influence of configuration-interactions and the contribution of crystal-field components of lower symmetry.

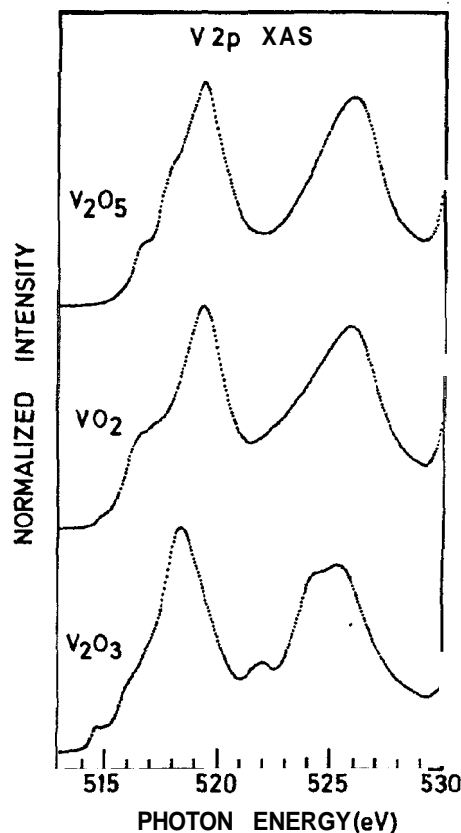


Figure 8: V 2p X-ray absorption spectra of V_2O_3 , VO_2 and V_2O_5 .

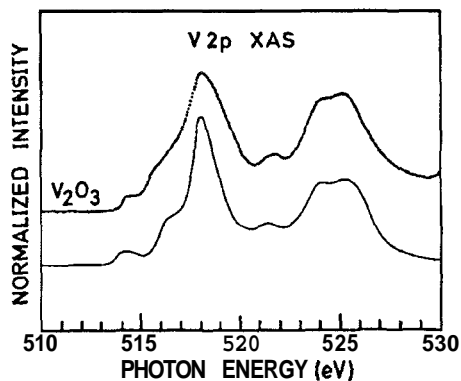


Figure 9: Comparison between the experimental V 2p X-ray absorption spectrum of V_2O_3 (dots) and an atomic-multiplet plus crystal-field simulation calculated by assuming a $t_{2g}^2(^3T_1)$ ground state with $10 Dq = 1.5$ eV (solid line).

D. Controlled-valence materials

Fig. 10 shows the V 2p X-ray absorption spectra of $\text{Li}_x\text{Zn}_{1-x}\text{V}_2\text{O}_4$ for different Li concentrations. The main question to be addressed here concerns the location of the holes induced by Li substitution in ZnV_2O_4 . In particular, whether the extra holes locate mainly at the vanadium or at the oxygen sites. Fig. 10 shows that the V 2p XAS spectra shift to higher photon energies as Zn is replaced by Li. This chemical shift indicates clearly that the formal valence of the vanadium ions is increasing. The shape of the multiplets in the V 2p XAS spectra changes also for higher Li concentrations. These changes are related to a decrease in the vanadium 3d-count which affects the symmetry of the ground state. Both effects indicate that the holes induced by Li substitution in ZnV_2O_4 contain mainly vanadium character. This conclusion can be confirmed by comparing the experimental V 2p XAS spectra to theoretical simulations.

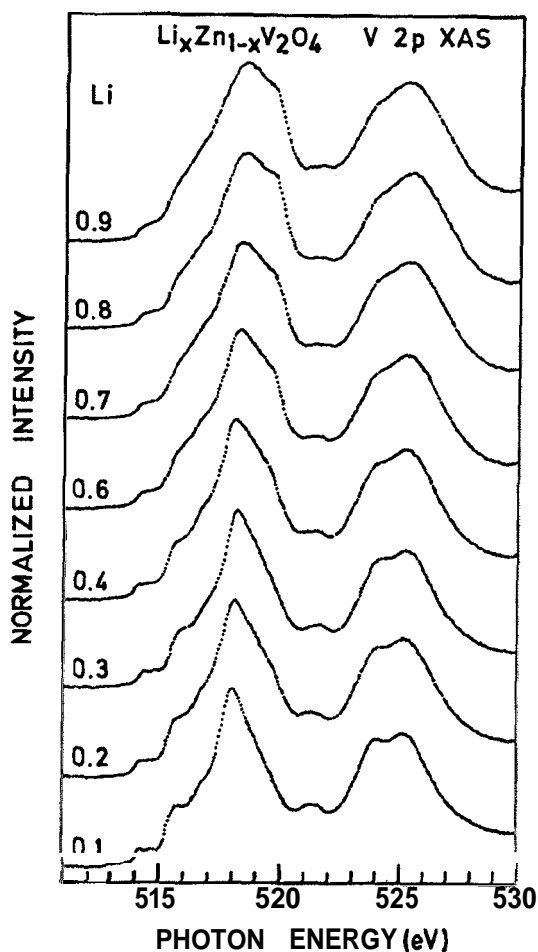


Figure 10: V 2p X-ray absorption spectra of $\text{Li}_x\text{Zn}_{1-x}\text{V}_2\text{O}_4$ for different Li concentrations.

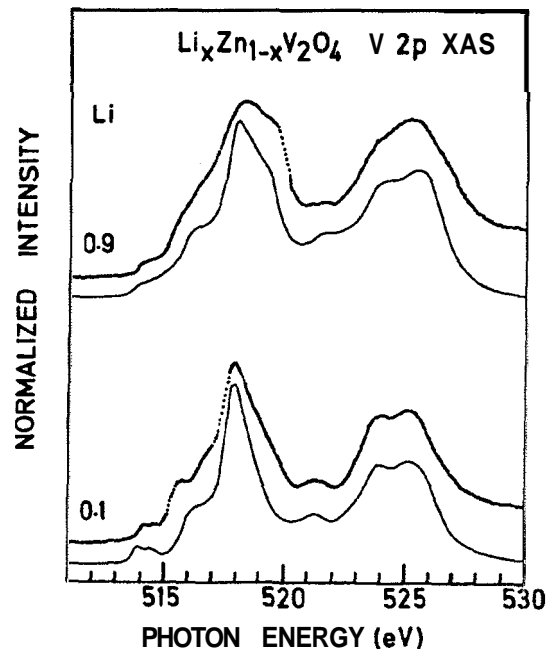


Figure 11: Comparison between the experimental V 2p X-ray absorption spectra of $\text{Li}_x\text{Zn}_{1-x}\text{V}_2\text{O}_4$ (dots) and atomic-multiplet plus crystal-field simulations (solid lines). The Zn-rich XAS spectrum (below) was simulated by assuming a t_{2g}^2 (3T_1) ground state with the 10 Dq parameter set to 1.5 eV. The Li-rich XAS spectrum (above) was simulated by assuming a mixed t_{2g}^2 (3T_1) and t_{2g}^1 (2T_2) ground state with the 10 Dq parameter set to 1.5 eV and 2.4 eV respectively.

Fig. 11 compares the experimental and theoretical V 2p X-ray absorption spectra of $\text{Li}_x\text{Zn}_{1-x}\text{V}_2\text{O}_4$ for both the Zn-rich and the Li-rich samples. In the Zn-rich sample, the experimental spectrum resembles very well the theoretical simulation calculated by assuming a t_{2g}^2 (3T_1) ground state (10 Dq = 1.5 eV). This comparison shows convincingly that the main contribution to the ground state of ZnV_2O_4 is $3d^2$. On the other hand, the spectrum of the Li-rich sample can be simulated fairly well by assuming a mixture of t_{2g}^2 (3T_1) and t_{2g}^1 (2T_2) states (10 Dq = 1.5 eV and 2.4 eV respectively). This simulation shows that the ground state of the Li-rich sample contains both $3d^2$ and $3d^1$ components and confirms again that the holes induced by Li substitution in ZnV_2O_4 located predominantly at the vanadium sites.

This kind of behavior upon hole doping is characteristic of most early transition-metal oxides. By contrast, the XAS spectra of most late transition-metal oxides exhibit only minor changes upon hole doping. This indicates that the metal 3d-count hardly change and, con-

Table I: Removal and addition states of a material with a $3d^n$ ground state according to the Anderson impurity model. The different possibilities are classified according to the relative value of the Mott-Hubbard parameter U and the charge-transfer energy Δ .

	Ground state	Removal state	Addition state
$U < \Delta$	$3d^n$	$3d^{n-1}$	$3d^{n+1}$
$U > \Delta$	$3d^n$	$3d^n \underline{L}$	$3d^{n+1}$
$U \approx \Delta$	$3d^n$	Mixed	$3d^{n+1}$

sequently, the holes induced by substitution are located primarily at the oxygen site^[50,51]. Finally, the holes induced by substitution in intermediate transition-metal oxides present a mixed metal-oxygen character.

The differences upon hole doping for early and late transition-metal oxides can be rationalized within the framework of the Anderson impurity model^[52-54]. This model is applied to the parent compound and gives the relative ordering of the different energy levels in terms of the Mott-Hubbard parameter U ^[55,56] and the charge-transfer energy Δ ^[57]. The Mott-Hubbard parameter corresponds to a 3d-3d charge fluctuation whereas the charge-transfer energy corresponds to a 2p-3d transfer. The first removal and addition states of a solid with a $3d^n$ ground state predicted by this model are summarized in Table I. The different possibilities are classified according to the relative value of U and Δ .

For low doping concentration, the holes induced by substitution will go to the first removal state (FRS) of the solid. There are three different possibilities according to the classification scheme provided by the Anderson impurity model:

- In late transition-metal oxides like $\text{Li}_x\text{Ni}_{1-x}\text{O}$, U is usually larger than Δ and the FRS will be mainly $3d^n \underline{L}$. This means that the holes induced by Li substitution in NiO contain mainly oxygen character.
- In early transition-metal oxides like smaller $\text{Li}_x\text{Zn}_{1-x}\text{V}_2\text{O}_4$, U is often smaller than Δ and the FRS will be mostly $3d^{n-1}$. This means that the holes induced by Li substitution in ZnV_2O_4 are located mainly at the metal sites.
- In intermediate transition-metal oxides like $\text{La}_{1-x}\text{Sr}_x\text{MnO}_3$, U is approximately equal to Δ

Table II: Main character of the ground state of the parent compound and the hole-doped state of the corresponding controlled-valence material for different transition-metal ions.

Parent compounds	Ground state	Doped compounds	Doped state
LaTiO_3	$3d^1$	$\text{La}_{1-x}\text{Sr}_x\text{TiO}_3$	$3d^n$
ZnV_2O_4	$3d^2$	$\text{La}_x\text{Zn}_{1-x}\text{V}_2\text{O}_4$	$3d^1$
LaCrO_3	$3d^3$	$\text{La}_{1-x}\text{Sr}_x\text{CrO}_3$	$3d^2 \underline{L}$
LaMnO_3	$3d^4$	$\text{La}_{1-x}\text{Sr}_x\text{MnO}_3$	$3d^3 + 3d^4 \underline{L}$
LaFeO_3	$3d^5$	$\text{La}_{1-x}\text{Sr}_x\text{FeO}_3$	$3d^5 \underline{L}$
LaCO_3	$3d^6$	$\text{La}_{1-x}\text{Sr}_x\text{CoO}_3$	$3d^5 + 3d^6 \underline{L}$
NiO	$3d^8$	$\text{La}_x\text{Ni}_{1-x}\text{O}$	$3d^8 \underline{L}$
La_2CuO_4	$3d^9$	$\text{La}_{2-x}\text{Sr}_x\text{CuO}_4$	$3d^9 \underline{L}$

and the FRS will be a mixture of $3d^{n-1}$ and $3d^n \underline{L}$. This means that the holes induced by Sr substitution in LaMnO_3 contain mixed metal-oxygen character.

In conclusion, the contrasting behavior upon hole doping for early and late transition-metal oxides is the natural consequence of the changes in the relative magnitude of U and Δ in the parent compounds. The ground state of the parent compound and the hole doped state of the corresponding controlled-valence material for different transition-metal ions are given in Table II.

V. Summary and conclusions

In summary, we presented and discussed the O 1s and V 2p X-ray absorption spectra of several vanadium oxides. The O 1s XAS spectra provide information on crystal-field effect, metal-ligand hybridization and the dispersion of the V 3d bands. The O 1s spectrum of metallic VO_2 can be explained by a symmetry-projected density of states. The O 1s XAS spectra of VO_2 show clearly the splitting of the V 3d bands across the semiconductor-metal transition. The shape of the multiplets in the V 2p XAS spectra are related to the symmetry and spin of the ground state. The V 2p XAS spectrum of V_2O_3 can be simulated by an atomic-multiplet calculation projected in the appropriate crystal-field. The V 2p XAS spectra of $\text{Li}_x\text{Zn}_{1-x}\text{V}_2\text{O}_4$ show that the holes induced by Li substitution in ZnV_2O_4 contain mainly V 3d character. In conclusion, soft X-ray absorption spectroscopy is a

very useful tool in the study of the electronic structure of transition-metal oxides.

Acknowledgments

I would like to thank J. C. Fuggle, G. A. Sawatzky, A. Fujimori, C. T. Chen, G. Kaindi and J. E. Inglesfield for continuous support. This work was partially supported by Fundamenteel Onderzoek der Materie (FORI), Scheikundig Onderzoek Nederland (SON) and the European Community SCIENCE program.

References

1. A. F. Wells, *Structural Inorganic Chemistry* (Clarendon Press, Oxford, 1975).
2. D. Adler, *Rev. Mod. Phys.* 40, 714 (1968).
3. J. B. Goodenough, *Prog. Solid State Chem.* 5, 145 (1971).
4. N. F. Mott, *Metal-Insulator Transition*, (Taylor and Francis, London, 1974).
5. K. Kawakami, Y. Sakai and N. Tsuda, *J. Phys. Soc. Japan* 55, 3174 (1986).
6. F. Takagi, K. Kawakami, I. Maekawa, Y. Sakai and N. Tsuda, *J. Phys. Soc. Japan* 56, 444 (1987).
7. F. Takagi, K. Kawakami and N. Tsuda, *J. Phys. Soc. Japan* 57, 3119 (1988).
8. E. Caruthers, L. Kleinman and H. I. Zhang, *Pliys. Rev.* B7, 3753 (1973).
9. E. Caruthers and L. Kleinman, *Phys. Rev.* B7, 3760 (1973).
10. M. Gupta, A. J. Freeman and D. E. Ellis, *Phys. Rev.* B16, 3338 (1977).
11. C. Soimiers, R. de Groot, D. Kaplan and A. Zylbersztejn, *J. Phys. (Paris)* 36, L 157 (1975).
12. M. Gupta and D. E. Ellis, *Pliys. Rev.* B13, 3405 (1976).
13. A. Zylbersztejn and N. F. Mott, *Phys. Rev.* B11, 4383 (1975).
14. A. Holz, K. A. Penson and K. H. Bennemann, *Phys. Rev.* B16, 399 (1977).
15. D. Paquet and P. Leroux-Hugon, *Phys. Rev.* B22, 5284 (1980).
16. C. Blaaw and P. Leroux-Hugon, *J. Phys. C* 8, 459 (1975).
17. G. A. Sawatzky and D. Post, *Phys. Rev.* B20, 1546 (1979).
18. C. N. R. Rao, D. D. Sarma, S. Vasudevam and M. S. Hedge, *Proc. Royal Soc. (London) A* 367, 239 (1979).
19. K. Smith and V. E. Henrich, *Phys. Rev.* B38, 5965 (1988).
20. K. Smith and V. E. Henrich, *Phys. Rev.* B38, 9571 (1988).
21. S. Shin, S. Suga, M. Taniguchi, M. Fujisawa, H. Kanzaki, A. Fujimori, H. Daimon, Y. Ueda, K. Kosuge and S. Kachi, *Phys. Rev.* B41, 499 (1990).
22. M. Abbate, H. F. Pen, M. T. Czyzyk, F. M. F. de Groot, J. C. Fuggle, Y. J. Ma, C. T. Chen, F. Sette, A. Fujimori, Y. Ueda and K. Kosuge, *J. Electron Spec. Relat. Phenom.* 62, 185 (1993).
23. A. Fujimori, K. Kawakami and N. Tsuda, *Pliys. Rev. B* 38, 7889 (1988).
24. J. C. Fuggle and J. E. Inglesfield, *Unoccupied Electronic States*, (Springer, Berlin, 1992).
25. The transitions to unoccupied V 4s character in the V 2p XAS spectra are much weaker and can be neglected in a first approximation.
26. W. Gudat and C. Kunz, *Phys. Rev. Lett.* 29, 169 (1972).
27. M. Abbate, J. B. Goedkoop, F. M. F. de Groot, M. Grioni, J. C. Fuggle, S. Hofmann, H. Petersen and M. Sacchi, *Surf. Interface Anal.* 18, 65 (1992).
28. C. T. Chen, *Nucl. Instrum. Methods* A256, 595 (1987).
29. C. T. Chen and F. Sette, *Rev. Sci. Instrum.* 60, 1616 (1989).
30. M. Domke, T. Mandel, A. Puschmann, C. Xue, D. A. Shirley, G. Kaindi, H. Petersen and P. Kuske, *Rev. Sci. Instrum.* 63, 80 (1992).
31. M. Pedio, J. C. Fuggle, J. Sommers, E. Umbach, J. Hasse, Th. Lindner, U. Hofer, M. Grioni, F. M. F. de Groot, B. Hillert, L. Becker and A. Robinson, *Pliys. Rev. B* 40, 7924 (1989).
32. D. W. Fischer, *J. Appl. Phys.* 41, 3561 (1970).
33. D. W. Fischer, *J. Phys. Chem. Solids* 32, 2455 (1971).
34. D. W. Fischer, *Pliys. Rev.* B5, 4219 (1972).

35. C. J. Ballhausen, *Introduction to Ligand Field Theory*, (MacGraw Hill, New York, 1962).
36. B. N. Figgis, *Introduction to Ligand Fields*, (Wiley, New York, 1966).
37. The contributions to the broadening coming from the O 1s core-hole lifetime, phonon effects and the experimental resolution are much smaller and can be neglected in a first approximation.
38. H. van Leuken, A. Lodder, M. T. Czyzyk, F. Springelkamp and R. A. de Groot, *Phys. Rev. B* **41**, 5613 (1990).
39. M. Grioni, M. T. Czyzyk, F. M. F. de Groot, J. C. Fuggle and B. E. Watts, *Phys. Rev. B* **39**, 4886 (1989).
40. J. J. M. Michiels, M. Grioni and J. C. Fuggle, *J. Phys.: Condens. Matter* **4**, 6943 (1992).
41. M. Grioni, J. F. van Acker, M. T. Czyzyk and J. C. Fuggle, *Phys. Rev. B* **45**, 3309 (1992).
42. M. Abbate, F. M. F. de Groot, J. C. Fuggle, Y. J. Ma, C. T. Chen, F. Sette, A. Fujimori, Y. Ueda and K. Kosuge, *Phys. Rev. B* **43**, 7263 (1991).
43. J. B. Goodenough, *J. Solid State Chem.* **3**, 490 (1971).
44. J. Taftø and O. L. Krivanek, *Phys. Rev. Lett.* **48**, 56C (1982).
45. G. van der Laan, B. T. Thole, G. A. Sawatzky and M. Verdaguer, *Phys. Rev. B* **37**, 6587 (1988).
46. F. M. F. de Groot, J. C. Fuggle, B. T. Thole and G. A. Sawatzky, *Phys. Rev. B* **41**, 928 (1990).
47. F. M. F. de Groot, J. C. Fuggle, B. T. Thole and G. A. Sawatzky, *Phys. Rev. B* **42**, 5459 (1990).
48. M. Abbate, F. M. F. de Groot, J. C. Fuggle, A. Fujimori, Y. Tokura, Y. Fujishima, O. Strebel, M. Domke, G. Kaindl, J. van Elp, B. T. Thole, G. A. Sawatzky, M. Sacchi and N. Tsuda, *Phys. Rev. B* **44**, 5419 (1991).
49. M. Abbate, F. M. F. de Groot, J. C. Fuggle, A. Fujimori, O. Strebel, F. Lopez, M. Domke, G. Kaindl, G. A. Sawatzky, M. Takano, Y. Takeda, H. Eisaki and S. Uchida, *Phys. Rev. B* **46**, 4511 (1992).
50. P. Kuiper, G. Kruizinga, J. Glijsen and G. A. Sawatzky, *Phys. Rev. Lett.* **62**, 221 (1989).
51. P. Kuiper, J. van Elp, G. A. Sawatzky, A. Fujimori, S. Hosoya and D. M. de Leeuw, *Phys. Rev. B* **44**, 4570 (1991).
52. J. Zaanen, G. A. Sawatzky and J. W. Allen, *Phys. Rev. Lett.* **55**, 418 (1985).
53. J. Zaanen, G. A. Sawatzky and J. W. Allen, *J. Mag. Mag. Materials* **54**, 607 (1986).
54. J. Zaanen and G. A. Sawatzky, *Can. J. Phys.* **65**, 1262 (1987).
55. N. F. Mott, *Proc. Royal Soc. (London) A* **62**, 416 (1949).
56. J. Hubbard, *Proc. Royal Soc. (London) A* **276**, 238 (1963).
57. G. van der Laan, C. Westra, C. Haas and G. A. Sawatzky, *Phys. Rev. B* **23**, 4329 (1981).